Supplement of

Ensemble estimates of global wetland methane emissions over 2000-2020

Zhen Zhang et al.

Correspondence to: Zhen Zhang (yuisheng@gmail.com)

Figures

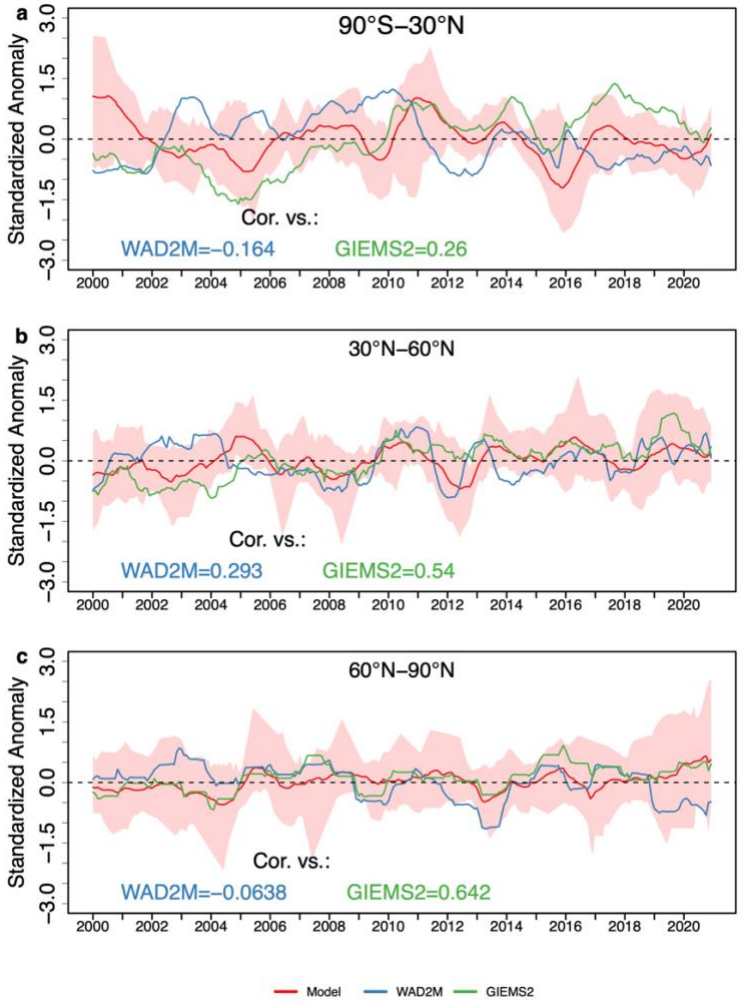

Figure S1. Temporal variations in wetland anomalies in model ensemble in comparison with satellite-based products WAD2M and GIEMS2. The wetland areal anomalies were calculated relative to the mean of 2000-2006 level and then standardized using a Z score. The shaded areas are the 1-standard deviation of model ensemble estimates. The solid lines are the 12-month running means of the anomalies. The correlations in the trend between model ensemble mean and satellite-based products are listed.

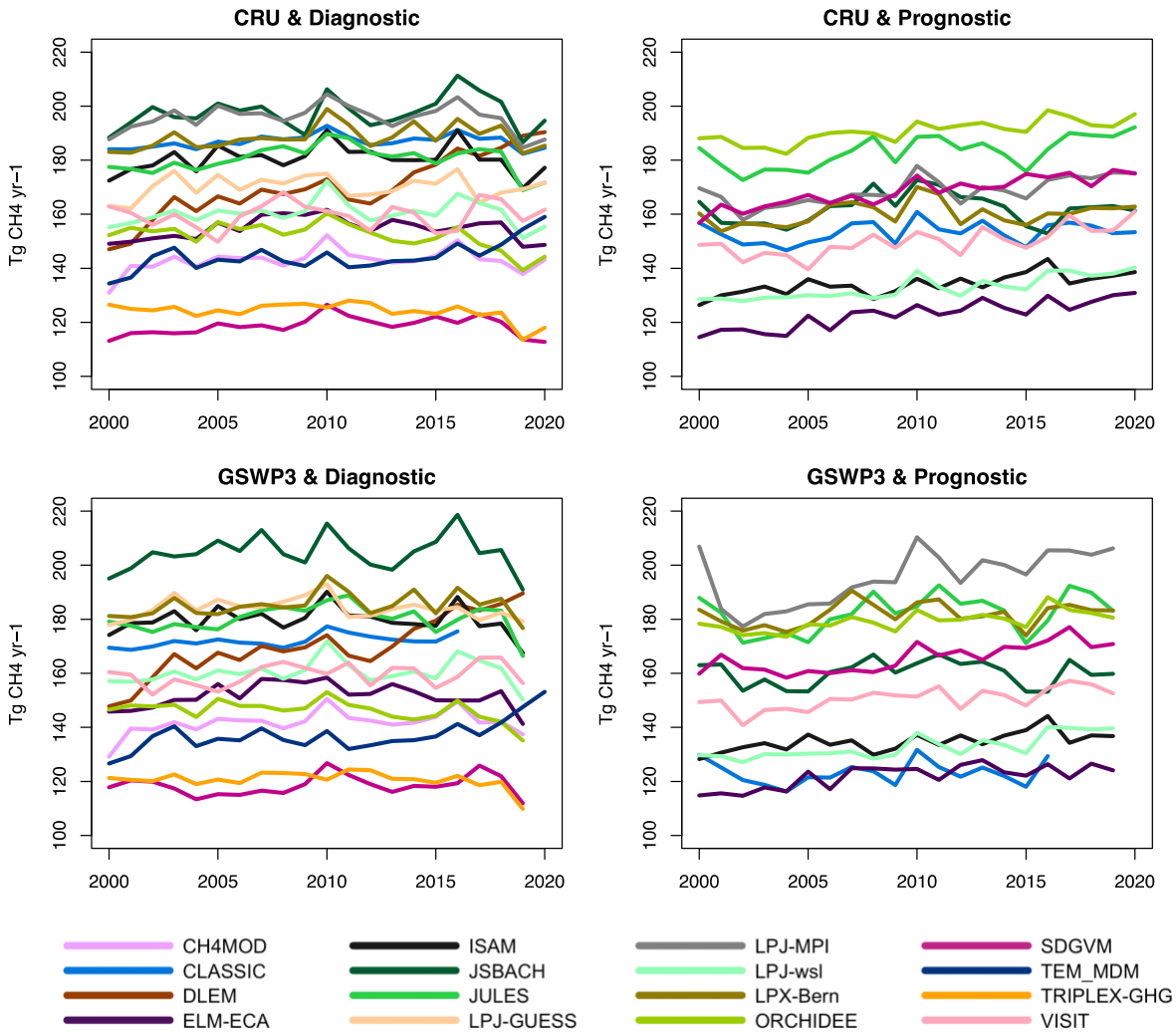

Figure S2. Time series of annual total CH_4 emissions from the prognostic runs. Note that 11 of the 16 models have prognostic estimates. Note that the diagnostic results are not used in interpreting temporal changes due to a discontinuity issue in a few tropical hotspots, which exists in some of the models (see Methods).

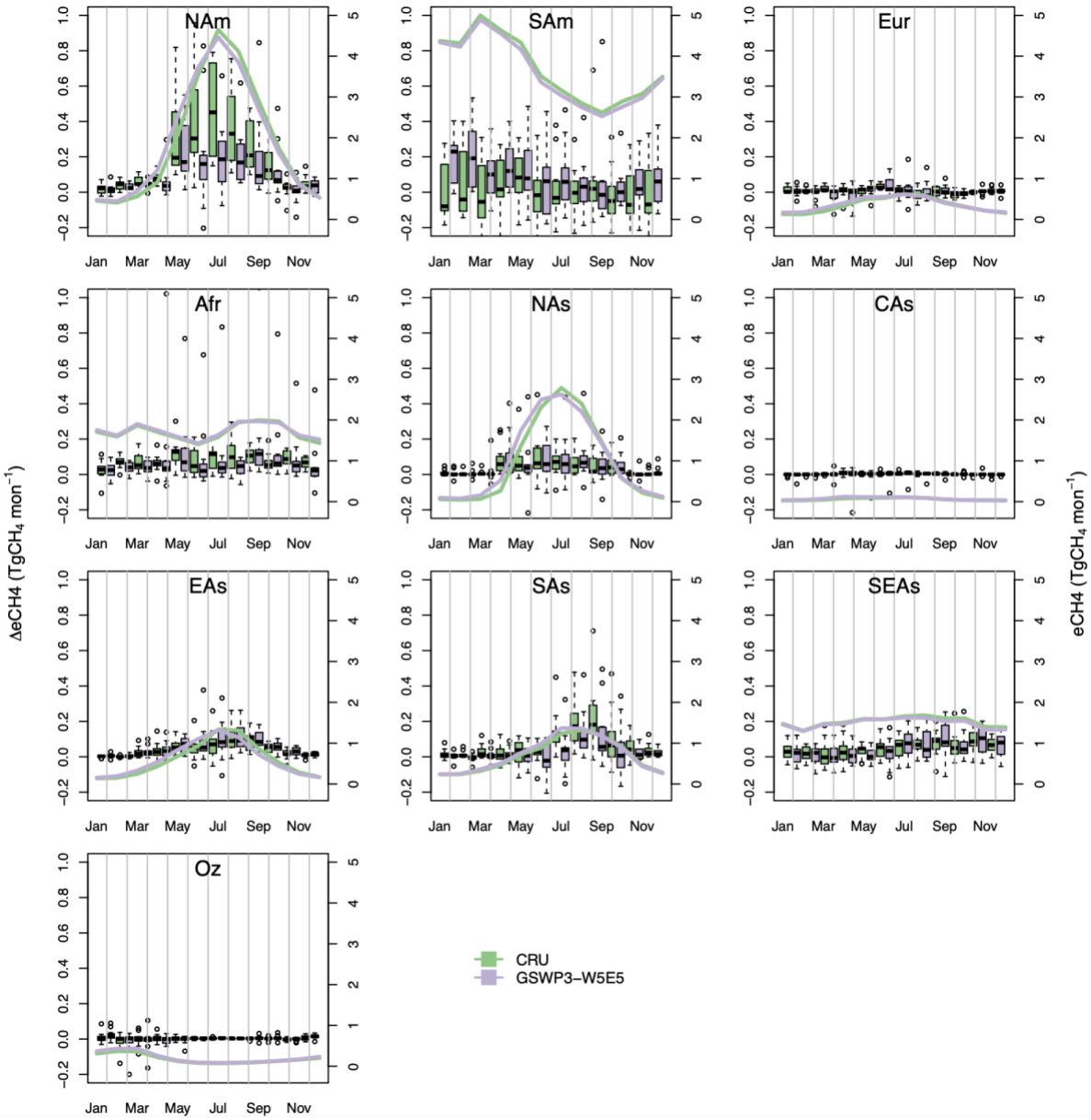
NAm
SAm
Eur
Afr
NAs
CAs
EAs
SAs
SEAs
Oz
Jan
Mar
May
Jul
Sep
Nov
ΔeCH4 (TgCH4 mon−1)
eCH4 (TgCH4 mon−1)
CRU
GSWP3−W5E5

Figure S3. Regional changes in the seasonal cycle of ΔeCH_4 and corresponding mean seasonal cycle. The boxplots represent mean ΔeCH_4 in the seasonal cycle during 2010-2019 relative to the average of 2000-2009. The black whiskers extend to the most extreme data points not considered outliers, which are denoted as dots. The colored lines represent the average seasonal cycle of 2000-2009 from the simulations grouped by two climate datasets, CRU and GSWP3-W5E5. Region Abbreviations: NAm, North America; SAm, South America; Eur, Europe; Afr, Africa; NAs, North Asia; CAs, Central Asia, EAs, East Asia; Sas, South Asia; SEAs, Southeast Asia; Oz, Oceania.

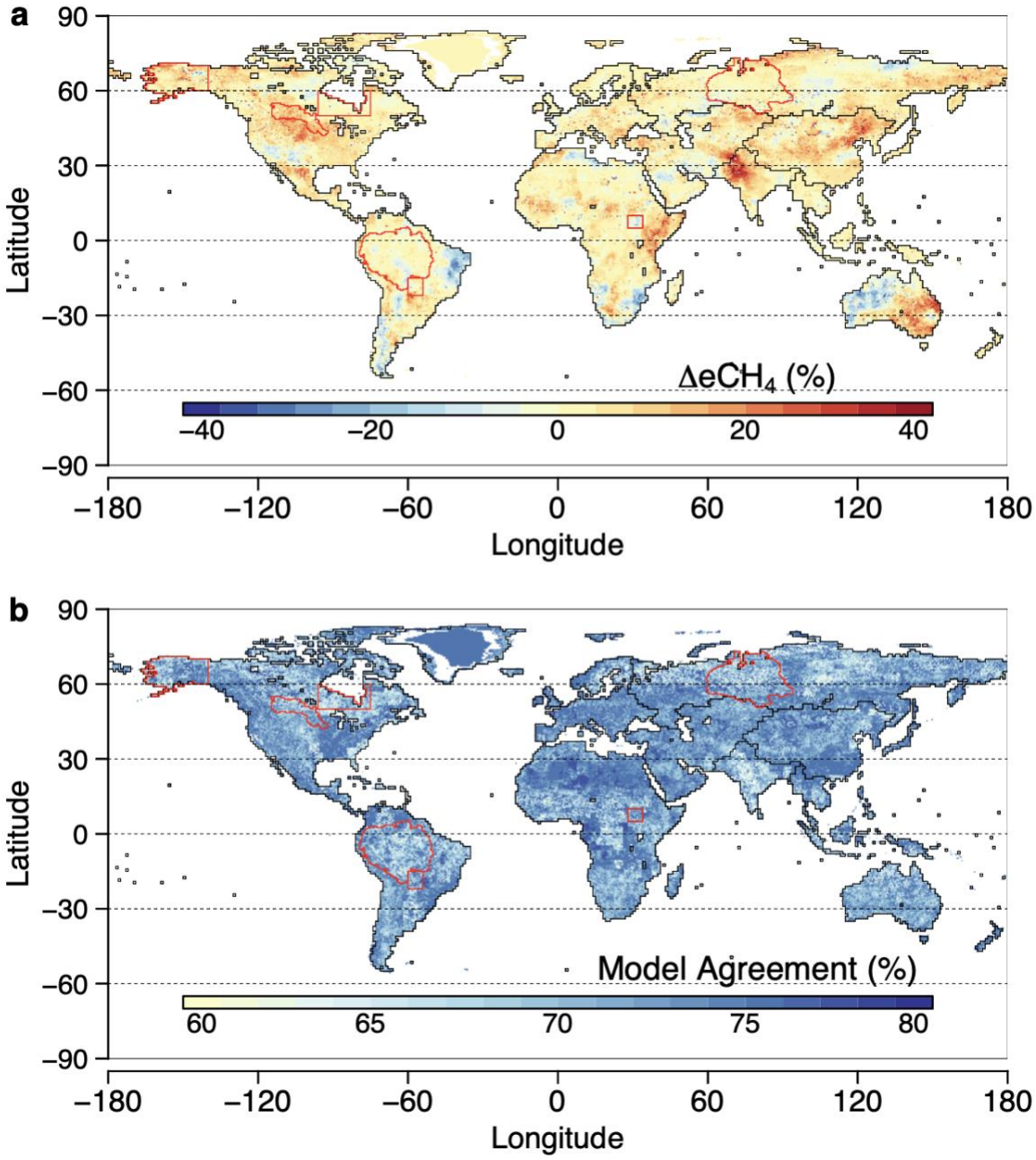
a
90
60
30
0
−30
−60
−90
Latitude
ΔeCH4 (%)
−40
−20
0
20
40
−180
−120
−60
0
60
120
180
Longitude
b
90
60
30
0
−30
−60
−90
Latitude
Model Agreement (%)
60
65
70
75
80
−180
−120
−60
0
60
120
180
Longitude

Figure S4. Spatial distribution of ΔeCH₄ in percentage between the 2010s and 2000s and the level of model agreement. The level of model agreement (%) is defined as the ratio of the number of runs whose estimates fall within the 1-σ range of the whole ensemble to the number of total runs (n=22). The regional CH₄ hotspots in Table S3 are shown in red.

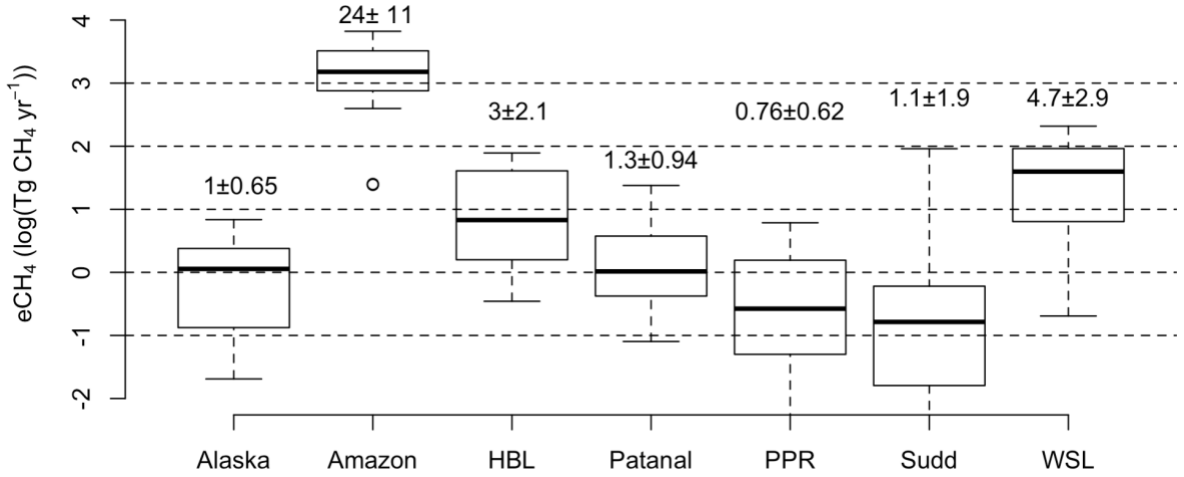

Figure S5. Boxplot of mean eCH₄ for regional hotspots from the prognostic runs. The model ensemble means are shown with one standard deviation for 2000-2020. The mask map is shown in Fig. S3. HBL, PPR, and WSL refer to 'Hudson Bay Lowland', 'Prairie Pothole Region', and 'West Siberian Lowland', respectively.

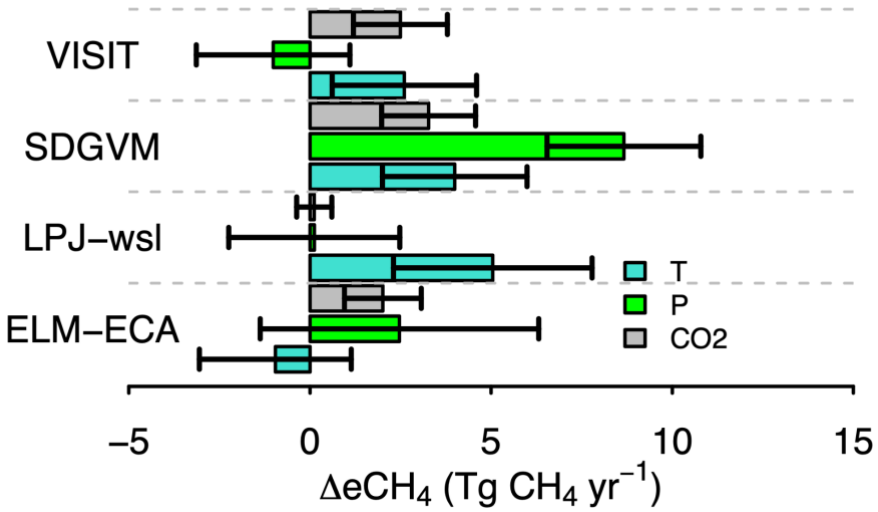

Figure S6. Attribution of mean ΔeCH_4 to the temperature (T), precipitation (P), and rising atmospheric CO_2 concentration (CO_2) based on factorial simulations of a subset of the models.

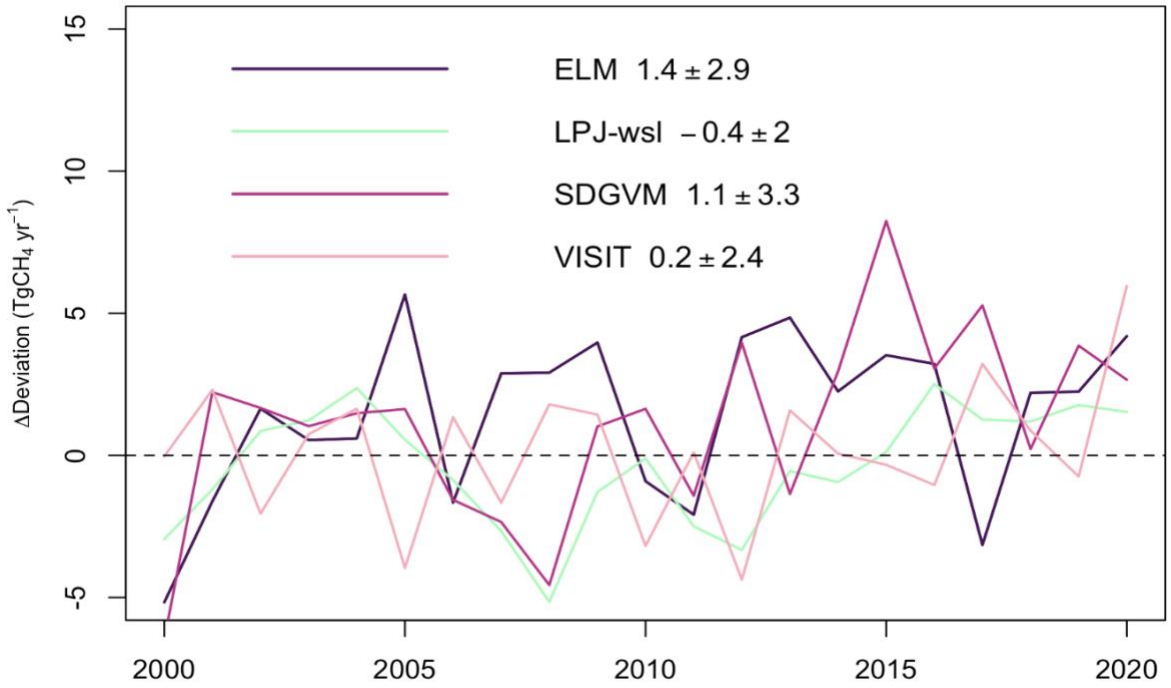

Figure S7. Time series of differences in eCH_4 between the subset of models from the factorial experiments and the annual mean from the full model ensemble. The mean deviation and one standard deviation are shown in the figure.

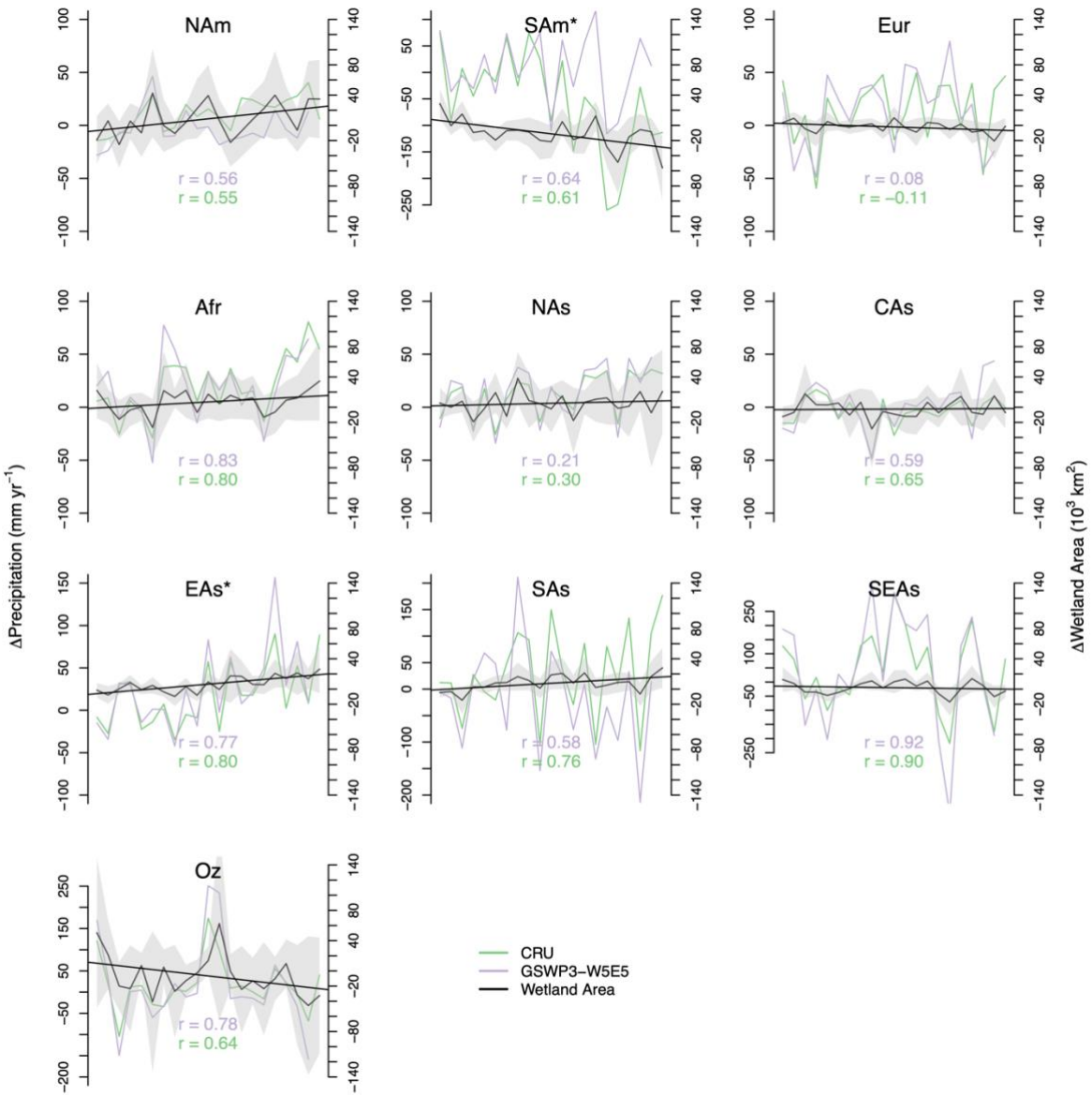
NAm
r = 0.56
r = 0.55
SAm*
r = 0.64
r = 0.61
Eur
r = 0.08
r = −0.11
Afr
r = 0.83
r = 0.80
NAs
r = 0.21
r = 0.30
CAs
r = 0.59
r = 0.65
EAs*
r = 0.77
r = 0.80
SAs
r = 0.58
r = 0.76
SEAs
r = 0.92
r = 0.90
Oz
r = 0.78
r = 0.64
CRU
GSWP3−W5E5
Wetland Area
ΔPrecipitation (mm yr−1)
ΔWetland Area (10^3 km^2)

Figure S8. Temporal variations of anomaly in precipitation and wetland area relative to the average of 2000-2006 over global wetlands. The precipitation inputs from CRU and GSWP3-W5E5, along with the ensemble mean of simulated wetland areas (black line) with its 1-σ uncertainty (grey area) derived from eighteen prognostic estimates by the wetland models, are presented. The statistically significant linear regional trends in wetland area are denoted with a star next to the region name. The Spearman correlations between precipitation and wetland area across regions are indicated in color corresponding to different precipitation inputs. The wetland mask is defined by maximum areal extent of the wetland product WAD2M. Region Abbreviations: NAm, North America; SAm, South America; Eur, Europe; Afr, Africa; NAs, North Asia; CAs, Central Asia, EAs, East Asia; Sas, South Asia; SEAs, Southeast Asia; Oz, Oceania.

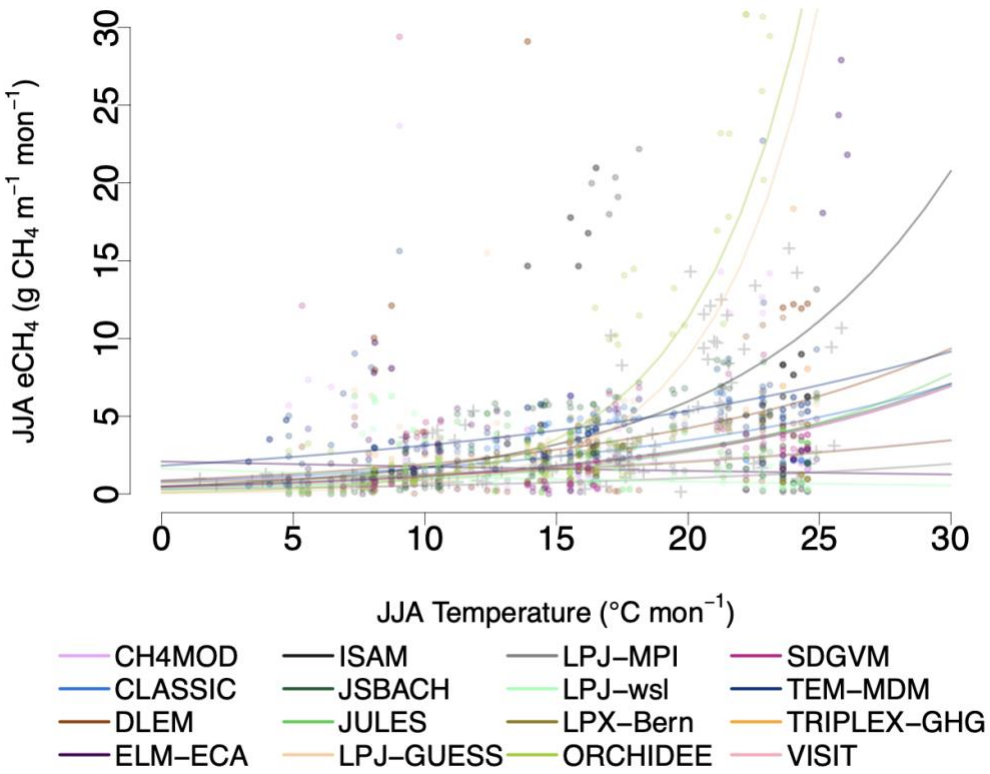

Figure S9. Temperature sensitivity of simulated seasonal eCH_4 across locations of FLUXNET-CH_4 sites from individual models for the JJA season.

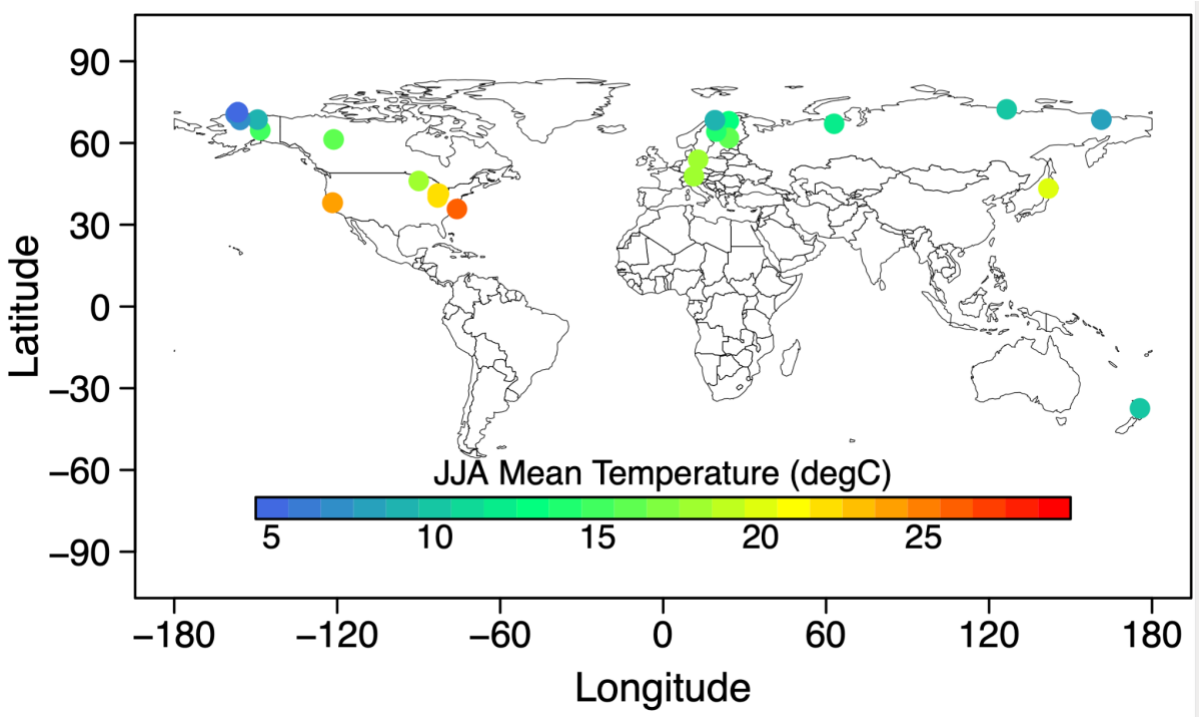

Figure S10. Map of FLUXNET-CH_4 sites applied in the Q_{10} calculation. The color of the points (n = 34) represents the average JJA temperature for 2000-2020 for each site. The site info can be found at Table S4.

Tables

Table S1. List of GCP-CH4 participating wetland models. Not all models contributed results to all experiments. The details on the model set-ups and models' methane flux parameterizations can be found in principal references.

Model	Wetland PFT	Components of CH_4 Flux	CH_4 Transport Pathway	Temperature Response Functions	CH_4 Production Proxy	Nitrogen Cycles	Fire	Spatial Resolution (deg)	Forcing Time Step	Reference
$CH4MOD_{wetland}$	Herbaceous wetland PFTs and Woody wetland	Net flux	Ebullition and Diffusion, and Plant mediated transport	Layered soil temperature	Carbon Substrate	No	No	0.5	Monthly	Li et al., 2020

	PFTs									
CLASSIC	No wetland-specific PFTs	Net flux	No specific transport pathways	Indirectly through Rh (see Section A3.2 in Melton and Arora 2016	Rh is scaled to account for CH_4 vs. CO_2 emitted and differences in upland vs. lowland Rh	No	Yes	T63 (~2.8)	30 minutes	Arora et al., 2018
DLEM	Generic wetland PFTs	gross production; gross consumption; oxidation;	No specific transport pathways	Layered soil temperature	Carbon Substrate	Yes	No	0.5	Daily	Tian, 2015; Tian et al., 2016
ELM-ECA	No wetland-specific PFTs	gross production; gross consumption; oxidation; diffusive, aerenchyma, and ebullition fluxes	Ebullition and Diffusion, and Plant mediated transport	Q10 based on soil T in each soil layer	Rh in each soil layer is scaled to estimate CH4 production	Yes	Yes	~2°	6-Hourly	Zhu et al., 2016;2019
ISAM	Upland PFTs, generic wetland PFTs, and Woody wetland PFTs	gross production, oxidation,	Ebullition and Diffusion		Heterotrophic respiration	Yes	No	0.5	6-Hourly	Shu 2020. Xu 2021.
JSBACH	Generic wetland PFT with C3 grass parameters for vegetation	gross production, oxidation	Ebullition and Diffusion, and Plant mediated transport	Layered soil temperature, different temperature responses for production, consumption	CH4 production depends on anoxic respiration produced by YASSO soil carbon model modified to account for anoxic conditions and coupled to JSBACH	No	No	1.875°	Daily	Kleinen et al., 2020; 2021.
JULES	No wetland-specific PFTs	Net fluxes	No specific transport pathways	Layered soil temperature	Net Primary Production	No	No	0.5	Daily	Clark 2011. Gedney 2019
LPJ-MPI	Upland PFTs, non-vascular PFTs, Hebaceous wetland PFTs	gross production and oxidation	Ebullition and Diffusion, and Plant mediated transport	Layered soil temperature, different temperature responses for production, consumption, diffusion	Heterotrophic respiration	No	Yes	0.5	Monthly	Kleinen et al., 2012
LPJ-wsl	No wetland-specific PFTs	net flux	No specific transport pathways	Soil temperature calculation in LPJ is 12 layers scheme following Wania et al., (2009). Daily average soil temperature for 0-50 cm depth is used for CH4 function.	Heterotrophic respiration	No	Yes	0.5	Monthly	Zhang et al., 2016, 2018
LPJ-GUESS	High-latitude (> 40°N): Wetland grass, cushion forbs, lichens, sphagnum moss. South of 40°N: C3 and C4 grasses only on wetlands	Net and gross emissions are simulated for high-latitude (> 40°N) ecosystems. South of 40°N: net emissions only based on a simple rescaling of heterotrophic respiration.	Diffusion, plant-mediated, and ebullition pathways for > 40N	Decomposition of litter and SOM uses an empirical relationship for temperature response of soil temperature at 25 cm depth (calculated following Wania et al., (2009a)) across ecosystems, incorporating damping of Q10 response due to temperature acclimation. CH_4	CH_4 production depends on soil temperature in each 10 cm soil layer, the degree of anoxia and the availability of substrate that consists of a fraction of litter and	Yes	No, not on wetlands	0.5	Monthly, interpolated to quasi-daily values	McGuire et al., 2012; Wania et al., 2010

				production, oxidation and transport use temperature dependencies from Wania et al. (2010), from each 10cm layer in the soil.	soil carbon decomposition					
LPX-Bern	wetland PFTs include non-vascular, Herbaceous wetland, and Woody wetland PFTs	gross production; gross consumption; net flux	Ebullition and Diffusion, and Plant mediated transport	Layered soil temperature, different temperature responses for production, consumption, diffusion	Heterotrophic respiration and carbon substrate	Yes	Yes	0.5	Monthly	Spahni et al., 2011; Stocker et al., 2014
ORCHIDEE	No wetland-specific PFTs	gross emission (gross production and oxidation) are simulated	Ebullition and Diffusion, and Plant mediated transport	Microbial activities are not represented directly. Only soil temperature and soil moisture which influence microbial activities are considered	Carbon Substrate	No	No	1	Daily	Ringeval et al., 2012; Guimberteau 2018
SDGVM	upland PFTs	Net flux	No specific transport pathways	Q10 coefficient using air temperature	Heterotrophic respiration	Yes	Yes	0.5	Monthly	SDGVM: Beerling & Woodward 2001;Fluxes following: Singarayer et al., 2011; Wetland area foloowing: Hopcroft et al., 2020
TEM-MDM	Five primary types of wetlands are considered in boreal, temperate and tropical regions (total 15 subtypes). They are forested bog, nonforested bog, forested swamp, nonforested swamp and alluvial formations	gross production; gross consumption; net flux	Ebullition and Diffusion, and Plant mediated transport	Q10 coefficient is used to account for soil temperature effects on methanotrophy rates within each 1 cm layer of the soil profile	CH_4 production is modeled as an anaerobic process that occurs in the saturated zone of the soil profile, controlled by methanogenic substrate availability, soil temperatures, PH, and redox potential.	Yes	No	0.5	Daily	Zhuang et al., 2004; Liu et al., 2020
VISIT	No wetland-specific PFTs	gross production; gross consumption; net flux;	Ebullition and Diffusion, and Plant mediated transport	Layered soil temperature.	Net Primary Production	No	Yes	0.5	Monthly	Ito and Inatomi, 2012; Ito et al., 2019
TRIPLEX-GHG	a general wetland PFT was added without considering	net flux	Ebullition and Diffusion, and Plant mediated transport	Soil temperature factor was evaluated with and exponential function that considering soil temperature and optimum soil	CH_4 production was calculated as a proportion of heterotrophic	Yes	No	0.5	Daily	(Zhu et al., 2015, 2017)

	specific wetland plants type			temperature for CH_4 production. The Q10 in the temperature function for CH_4 production and CH_4 oxidation could be calibrated separately.	respiration (CO2–C) along with soil temperature, Eh and pH modification factors					

Table S2. Factorial simulation setup for 2007-2020.

Simulation	Temperature	Precipitation	CO_2 concentration
Transient	varying	varying	varying
Baseline	climatology of 2000-2006	climatology of 2000-2006	2006 value
Temperature Fix run	climatology of 2000-2006	varying	varying
Precipitation Fix run	varying	climatology of 2000-2006	varying
CO_2 concentration Fix run	varying	varying	2006 value

Table S3. Modeled CH_4 emissions (Unit: $TgCH_4\ yr^{-1}$) and comparison with estimates from bottom-up (BU) and top-down (TD) studies for regional CH_4 hotspots.

Region	Emissions ($TgCH_4\ yr^{-1}$)	Method	Reference
Amazon	24±11	BU modeling	This study
	29	BU upscaling	Melack et al., 2004
	47.3-53.0	TD inversion*	Bergamaschi et al., 2009
	44±4.8	TD inversion*	Ringeval et al., 2014
	31.0-42.0	TD inversion*	Wilson et al., 2016
	35±5.6-41.7±5.9	BU upscaling*	Pangala et al., 2017
	38.2±5.3-45.6±5.2	TD inversion*	Wilson et al., 2021
	33.8±10.9	TD inversion*	Basso et al., 2021
	9.2±1.8	TD inversion	Tunnicliffe et al., 2020
	39.4±10.3	BU modeling	Bloom et al., 2017
HBL	3±2.1	BU modeling	This study
	2.3	TD inversion	Pickett-Heaps et al., 2011
WSL	4.7±2.9	BU modeling	This study
	6.1±1.2	TD inversion	Bohn et al., 2015
	5.3±0.5	BU modeling	Melton et al., 2013
	3.9±1.3	BU upscaling	Glagolev et al., 2011
Alaska	1.0±0.65	BU modeling	This study
	2.1±0.5	TD inversion	Chang et al., 2014
	1.7±0.3	TD inversion	Miller et al., 2016
Pantanal	1.3±0.94	BU modeling	This study
	3.3	BU upscaling	Marani and Alvalá, 2007
	2.1-3.6	BU modeling	Gerlein-Safdi et al., 2021
	2.0-2.8 or 3.3	TD inversion	Gloor et al., 2021

Sudd	1.1±1.9	BU modeling	This study
	1.1±0.5	BU modeling	Bloom et al., 2017
	2.5-7**	TD inversion	Lunt et al., 2019
	7.2±3.2**	TD inversion	Pandey et al., 2021
	2.1-3.6**	BU modeling	Gerlein-Safdi et al., 2021

* These numbers do not distinguish generic wetland applied in this study with the estimates from open water system (e.g., rivers, lakes, ponds, and reservoirs)

**These numbers are derived from a short time period (2017-2020) when the strong positive anomaly occurred at Sudd wetlands, while the model ensemble is average of 2000-2020 level.

Table S4. FLUXNET-CH_4 site used in the temperature dependence analysis.

Site ID	Site Name	Country	LAT	LON	Biome	Ecosystem Type	Site PIs	DOI/ Dataset
CA-Scb	Scotty Creek Bog	Canada	61.31	-121.30	Boreal Forests	Bog	Oliver Sonnentag	AmeriFlux
CA-Scc	Scotty Creek Peat plateau/collapse scar	Canada	61.31	-121.30	Boreal Forests	Peat plateau	Oliver Sonnentag	doi:10.17190/A MF/1480303
DE-Sfn	Schechenfilz Nord	Germany	47.81	11.33	Temperate	Bog	Hans Peter Schmid	European Fluxes Database Cluster
DE-Zrk	Zarnekow	Germany	53.88	12.89	Temperate	Fen	Torsten Sachs	European Fluxes Database Cluster
FI-Lom	Lompolojankka	Finland	68.00	24.21	Boreal Forests	Fen	Annalea Lohila, Mika Aurela	European Fluxes Database Cluster
FI-Si2	Siikaneva II	Finland	61.84	24.17	Boreal Forests	Bog	Timo Vesala & Ivan Mammarella	European Fluxes Database Cluster
FI-Sii	Siikaneva I	Finland	61.83	24.19	Boreal Forests	Fen	Timo Vesala & Ivan Mammarella	European Fluxes Database Cluster
JP-Bby	Bibai Mire	Japan	43.32	141.81	Temperate	Bog	Masahito Ueyama	European Fluxes Database Cluster
NZ-Kop	Kopuatai	New Zealand	-37.39	175.55	Temperate	Bog	Dave Campbell	https://researchcommons.waikato.ac.nz/handle/10 289/11393
RU-Ch2	Chersky reference	Russia	68.62	161.35	Boreal Forests	Wet tundra	Matthias Goeckede	European Fluxes Database Cluster
RU-Che	Chersky	Russia	68.61	161.34	Boreal Forests	Wet tundra	Matthias Goeckede	European Fluxes Database Cluster
RU-Sam	Samoylov	Russia	72.37	126.50	Tundra	Wet tundra	Torsten Sachs	European Fluxes Database Cluster
RU-Vrk	Seida/Vorkuta	Russia	67.06	62.94	Tundra	Wet tundra	Thomas Friborg	European Fluxes Database Cluster
SE-Deg	Degero	Sweden	64.18	19.56	Boreal Forests	Fen	Mats Nilsson	European Fluxes Database Cluster
SE-St1	Stordalen grassland (Mire)	Sweden	68.35	19.05	Tundra	Fen	Thomas Friborg	European Fluxes Database Cluster
SE-Sto	Stordalen Palsa Bog	Sweden	68.36	19.05	Tundra	Bog	Thomas Friborg	European Fluxes Database Cluster
US-Atq	Atqasuk	USA	70.47	-157.41	Tundra	Wet tundra	Donatella Zona	doi:10.17190/A MF/1246029
US-Beo	Barrow	USA	71.28	-156.61	Tundra	Wet tundra	Donatella Zona	AmeriFlux
US-Bes	Barrow	USA	71.28	-156.6	Tundra	Wet tundra	Donatella Zona	AmeriFlux
US-Bgl	Bog Lake peatland	USA	47.53	-93.74	Temperate	Fen	Narasinha Shurpali	AmeriFlux
US-Bzb	Thermokarst collapse bog	USA	64.70	-148.32	Boreal Forests	Bog	Eugenie Euskirchen	AmeriFlux
US-Bzf	Rich Fen	USA	64.70	-148.31	Boreal Forests	Fen	Eugenie Euskirchen	AmeriFlux

US-Ics	Wet sedge tundra	USA	68.61	-149.31	Tundra	Wet tundra	Eugenie Euskirchen	doi: 10.17190/AM F/1246130
US-Ivo	Ivotuk	USA	68.49	-155.75	Tundra	Wet tundra	Donatella Zona	doi:10.17190/A MF/1246067
US-Los	Lost Creek	USA	46.08	-89.98	Temperate	Fen	Ankur Desai	doi: 10.17190/AM F/1246071
US-Myb	Mayberry Wetland	USA	38.05	-121.77	Temperate	Marsh	Dennis Baldocchi	doi: 10.17190/AM F/1246139
US-NC4	NC Alligator River	USA	35.79	-75.90	Temperate	Swamp	Asko Noormets	doi:10.17190/A MF/1480314
US-Ngb	NGEE Barrow	USA	71.28	-156.61	Tundra	Wet tundra	Margaret Torn	doi: 10.17190/AM F/1436326
US-ORv	River Wetland Research Park	USA	40.02	-83.02	Temperate	Marsh	Gil Bohrer	doi:10.17190/A MF/1246135
US-Owc	Old Woman Creek	USA	41.38	-82.51	Temperate	Marsh	Gil Bohrer	doi: 10.17190/AM F/1246094
US-Sne	Sherman Island Restored Wetland	USA	38.04	-121.76	Temperate	Marsh	Dennis Baldocchi	doi: 10.17190/AM F/1418684
US-Tw1	Twitchell West Pond Wetland	USA	38.11	-121.65	Temperate	Marsh	Dennis Baldocchi	doi: 10.17190/AM F/1246147
US-Tw4	Twitchell East End Wetland	USA	38.10	-121.64	Temperate	Marsh	Dennis Baldocchi	doi: 10.17190/AM F/1246148
US-Wpt	Winous Point North Marsh	USA	41.46	-83.00	Temperate	Marsh	Housen Chu	doi: 10.17190/AM F/1246155

References

Arora, V. K., Melton, J. R., and Plummer, D.: An assessment of natural methane fluxes simulated by the CLASS-CTEM model, Biogeosciences, 15, 4683–4709, https://doi.org/10.5194/bg-15-4683-2018, 2018.

Basso, L. S., Marani, L., Gatti, L. V., Miller, J. B., Gloor, M., Melack, J., Cassol, H. L. G., Tejada, G., Domingues, L. G., Arai, E., Sanchez, A. H., Corrêa, S. M., Anderson, L., Aragão, L. E. O. C., Correia, C. S. C., Crispim, S. P., and Neves, R. A. L.: Amazon methane budget derived from multi-year airborne observations highlights regional variations in emissions, Commun Earth Environ, 2, 1–13, https://doi.org/10.1038/s43247-021-00314-4, 2021.

Bloom, A. A., Bowman, K. W., Lee, M., Turner, A. J., Schroeder, R., Worden, J. R., Weidner, R., McDonald, K. C., and Jacob, D. J.: A global wetland methane emissions and uncertainty dataset for atmospheric chemical transport models (WetCHARTs version 1.0), Geoscientific Model Development, 10, 2141–2156, https://doi.org/10.5194/gmd-10-2141-2017, 2017.

Bohn, T. J., Melton, J. R., Ito, A., Kleinen, T., Spahni, R., Stocker, B. D., Zhang, B., Zhu, X., Schroeder, R., Glagolev, M. V., Maksyutov, S., Brovkin, V., Chen, G., Denisov, S. N., Eliseev, A. V., Gallego-Sala, A., McDonald, K. C., Rawlins, M. A., Riley, W. J., Subin, Z. M., Tian, H., Zhuang, Q., and Kaplan, J. O.: WETCHIMP-WSL: intercomparison of wetland methane emissions models over West Siberia, Biogeosciences, 12, 3321–3349, https://doi.org/10.5194/bg-12-3321-2015, 2015.

Chang, R. Y.-W., Miller, C. E., Dinardo, S. J., Karion, A., Sweeney, C., Daube, B. C., Henderson, J. M., Mountain, M. E., Eluszkiewicz, J., Miller, J. B., Bruhwiler, L. M. P., and Wofsy, S. C.: Methane emissions from Alaska in 2012 from CARVE airborne observations, Proceedings of the National Academy of Sciences, 111, 16694–16699, https://doi.org/10.1073/pnas.1412953111, 2014.

Gerlein-Safdi, C., Bloom, A. A., Plant, G., Kort, E. A., and Ruf, C. S.: Improving Representation of Tropical Wetland Methane Emissions With CYGNSS Inundation Maps, Global Biogeochemical Cycles, 35, e2020GB006890, https://doi.org/10.1029/2020GB006890, 2021.

Glagolev, M., Kleptsova, I., Filippov, I., Maksyutov, S., and Machida, T.: Regional methane emission from West Siberia mire landscapes, Environmental Research Letters, 6, 045214, https://doi.org/10.1088/1748-9326/6/4/045214, 2011.

Gloor, M., Gatti, L. V., Wilson, C., Parker, R. J., Boesch, H., Popa, E., Chipperfield, M. P., Poulter, B., Zhang, Z., Basso, L., Miller, J., McNorton, J., Jimenez, C., and Prigent, C.: Large Methane Emissions From the Pantanal During Rising Water-Levels Revealed by Regularly Measured Lower Troposphere CH4 Profiles, Global Biogeochemical Cycles, 35, e2021GB006964, https://doi.org/10.1029/2021GB006964, 2021.

Hopcroft, P. O., Ramstein, G., Pugh, T. A. M., Hunter, S. J., Murguia-Flores, F., Quiquet, A., Sun, Y., Tan, N., and Valdes, P. J.: Polar amplification of Pliocene climate by elevated trace gas radiative forcing, PNAS, 117, 23401–23407, https://doi.org/10.1073/pnas.2002320117, 2020.

Ito, A. and Inatomi, M.: Use of a process-based model for assessing the methane budgets of global terrestrial ecosystems and evaluation of uncertainty, Biogeosciences, 9, 759–773, https://doi.org/10.5194/bg-9-759-2012, 2012.

Ito, A., Tohjima, Y., Saito, T., Umezawa, T., Hajima, T., Hirata, R., Saito, M., and Terao, Y.: Methane budget of East Asia, 1990–2015: A bottom-up evaluation, Science of The Total Environment, https://doi.org/10.1016/j.scitotenv.2019.04.263, 2019.

Kleinen, T., Brovkin, V., and Schuldt, R. J.: A dynamic model of wetland extent and peat accumulation: results for the Holocene, Biogeosciences, 9, 235–248, https://doi.org/10.5194/bg-9-235-2012, 2012.

Li, T., Lu, Y., Yu, L., Sun, W., Zhang, Q., Zhang, W., Wang, G., Qin, Z., Yu, L., Li, H., and Zhang, R.: Evaluation of CH4MODwetland and Terrestrial Ecosystem Model (TEM) used to estimate global CH4 emissions from natural wetlands, Geosci. Model Dev., 13, 3769–3788, https://doi.org/10.5194/gmd-13-3769-2020, 2020.

Liu, L., Zhuang, Q., Oh, Y., Shurpali, N. J., Kim, S., and Poulter, B.: Uncertainty Quantification of Global Net Methane Emissions From Terrestrial Ecosystems Using a Mechanistically Based Biogeochemistry Model, Journal of Geophysical Research: Biogeosciences, 125, e2019JG005428, https://doi.org/10.1029/2019JG005428, 2020.

Lunt, M. F., Palmer, P. I., Feng, L., Taylor, C. M., Boesch, H., and Parker, R. J.: An increase in methane emissions from tropical Africa between 2010 and 2016 inferred from satellite data, Atmospheric Chemistry and Physics, 19, 14721–14740, https://doi.org/10.5194/acp-19-14721-2019, 2019.

Marani, L. and Alvalá, P. C.: Methane emissions from lakes and floodplains in Pantanal, Brazil, Atmospheric Environment, 41, 1627–1633, https://doi.org/10.1016/j.atmosenv.2006.10.046, 2007.

McGuire, A. D., Christensen, T. R., Hayes, D., Heroult, A., Euskirchen, E., Kimball, J. S., Koven, C., Lafleur, P., Miller, P. A., Oechel, W., Peylin, P., Williams, M., and Yi, Y.: An assessment of the carbon balance of Arctic tundra: comparisons among observations, process models, and atmospheric inversions, Biogeosciences, 9, 3185–3204, https://doi.org/10.5194/bg-9-3185-2012, 2012.

Melack, J. M., Hess, L. L., Gastil, M., Forsberg, B. R., Hamilton, S. K., Lima, I. B. T., and Novo, E. M. L. M.: Regionalization of methane emissions in the Amazon Basin with microwave remote sensing, Global Change Biology, 10, 530–544, https://doi.org/10.1111/j.1365-2486.2004.00763.x, 2004.

Melton, J. R., Wania, R., Hodson, E. L., Poulter, B., Ringeval, B., Spahni, R., Bohn, T., Avis, C. A., Beerling, D. J., Chen, G., Eliseev, A. V., Denisov, S. N., Hopcroft, P. O., Lettenmaier, D. P., Riley, W. J., Singarayer, J. S., Subin, Z. M., Tian, H., Zürcher, S., Brovkin, V., van Bodegom, P. M., Kleinen, T., Yu, Z. C., and Kaplan, J. O.: Present state of global wetland extent and wetland methane modelling: conclusions from a model inter-comparison project (WETCHIMP), Biogeosciences, 10, 753–788, https://doi.org/10.5194/bg-10-753-2013, 2013.

Miller, S. M., Miller, C. E., Commane, R., Chang, R. Y.-W., Dinardo, S. J., Henderson, J. M., Karion, A., Lindaas, J., Melton, J. R., Miller, J. B., Sweeney, C., Wofsy, S. C., and Michalak, A. M.: A multiyear estimate of methane fluxes in Alaska from CARVE atmospheric observations: METHANE FLUXES FROM ALASKA, Global Biogeochemical Cycles, 30, 1441–1453, https://doi.org/10.1002/2016GB005419, 2016.

Pandey, S., Houweling, S., Lorente, A., Borsdorff, T., Tsivlidou, M., Bloom, A. A., Poulter, B., Zhang, Z., and Aben, I.: Using satellite data to identify the methane emission controls of South Sudan's wetlands, Biogeosciences, 18, 557–572, https://doi.org/10.5194/bg-18-557-2021, 2021.

Pangala, S. R., Enrich-Prast, A., Basso, L. S., Peixoto, R. B., Bastviken, D., Hornibrook, E. R. C., Gatti, L. V., Marotta, H., Calazans, L. S. B., Sakuragui, C. M., Bastos, W. R., Malm, O., Gloor, E., Miller, J. B., and Gauci, V.: Large emissions from floodplain trees close the Amazon methane budget, Nature, 552, 230–234, https://doi.org/10.1038/nature24639, 2017.

Pickett-Heaps, C. A., Jacob, D. J., Wecht, K. J., Kort, E. A., Wofsy, S. C., Diskin, G. S., Worthy, D. E. J., Kaplan, J. O., Bey, I., and Drevet, J.: Magnitude and seasonality of wetland methane emissions from the Hudson Bay Lowlands (Canada), Atmospheric Chemistry and Physics, 11, 3773–3779, https://doi.org/10.5194/acp-11-3773-2011, 2011.

Ringeval, B., Decharme, B., Piao, S. L., Ciais, P., Papa, F., de Noblet-Ducoudré, N., Prigent, C., Friedlingstein, P., Gouttevin, I., Koven, C., and Ducharne, A.: Modelling sub-grid wetland in the ORCHIDEE global land surface model: evaluation against river discharges and remotely sensed data, Geoscientific Model Development, 5, 941–962, https://doi.org/10.5194/gmd-5-941-2012, 2012.

Ringeval, B., Houweling, S., van Bodegom, P. M., Spahni, R., van Beek, R., Joos, F., and Röckmann, T.: Methane emissions from floodplains in the Amazon Basin: challenges in developing a process-based model for global applications, Biogeosciences, 11, 1519–1558, https://doi.org/10.5194/bg-11-1519-2014, 2014.

Singarayer, J. S., Valdes, P. J., Friedlingstein, P., Nelson, S., and Beerling, D. J.: Late Holocene methane rise caused by orbitally controlled increase in tropical sources, Nature, 470, 82–85, https://doi.org/10.1038/nature09739, 2011.

Spahni, R., Wania, R., Neef, L., van Weele, M., Pison, I., Bousquet, P., Frankenberg, C., Foster, P. N., Joos, F., Prentice, I. C., and van Velthoven, P.: Constraining global methane emissions and uptake by ecosystems, Biogeosciences, 8, 1643–1665, https://doi.org/10.5194/bg-8-1643-2011, 2011.

Stocker, B. D., Spahni, R., and Joos, F.: DYPTOP: a cost-efficient TOPMODEL implementation to simulate sub-grid spatio-temporal dynamics of global wetlands and peatlands, Geoscientific Model Development Discussions, 7, 4875–4930, https://doi.org/10.5194/gmdd-7-4875-2014, 2014.

Tian, B.: Spread of model climate sensitivity linked to double-Intertropical Convergence Zone bias, Geophysical Research Letters, 42, 4133–4141, https://doi.org/10.1002/2015GL064119, 2015.

Tian, H., Lu, C., Ciais, P., Michalak, A. M., Canadell, J. G., Saikawa, E., Huntzinger, D. N., Gurney, K. R., Sitch, S., Zhang, B., Yang, J., Bousquet, P., Bruhwiler, L., Chen, G., Dlugokencky, E., Friedlingstein, P., Melillo, J., Pan, S., Poulter, B., Prinn, R., Saunois, M., Schwalm, C. R., and Wofsy, S. C.: The terrestrial biosphere as a net source of greenhouse gases to the atmosphere, Nature, 531, 225–228, https://doi.org/10.1038/nature16946, 2016.

Tunnicliffe, R. L., Ganesan, A. L., Parker, R. J., Boesch, H., Gedney, N., Poulter, B., Zhang, Z., Lavrič, J. V., Walter, D., Rigby, M., Henne, S., Young, D., and O'Doherty, S.: Quantifying sources of Brazil's CH4 emissions between 2010 and 2018 from satellite data, Atmos. Chem. Phys., 20, 13041–13067, https://doi.org/10.5194/acp-20-13041-2020, 2020.

Wania, R., Ross, I., and Prentice, I. C.: Implementation and evaluation of a new methane model within a dynamic global vegetation model: LPJ-WHyMe v1.3.1, Geoscientific Model Development, 3, 565–584, https://doi.org/10.5194/gmd-3-565-2010, 2010.

Wilson, C., Chipperfield, M. P., Gloor, M., Parker, R. J., Boesch, H., McNorton, J., Gatti, L. V., Miller, J. B., Basso, L. S., and Monks, S. A.: Large and increasing methane emissions from eastern Amazonia derived from satellite data, 2010–2018, Atmospheric Chemistry and Physics, 21, 10643–10669, https://doi.org/10.5194/acp-21-10643-2021, 2021.

Wilson, D., Farrell, C. A., Fallon, D., Moser, G., Müller, C., and Renou-Wilson, F.: Multiyear greenhouse gas balances at a rewetted temperate peatland, Global Change Biology, 22, 4080–4095, https://doi.org/10.1111/gcb.13325, 2016.

Zhang, Z., Zimmermann, N. E., Kaplan, J. O., and Poulter, B.: Modeling spatiotemporal dynamics of global wetlands: comprehensive evaluation of a new sub-grid TOPMODEL parameterization and uncertainties, Biogeosciences, 13, 1387–1408, https://doi.org/10.5194/bg-13-1387-2016, 2016.

Zhang, Z., Zimmermann, N. E., Calle, L., Hurtt, G., Chatterjee, A., and Poulter, B.: Enhanced response of global wetland methane emissions to the 2015–2016 El Niño-Southern Oscillation event, Environmental Research Letters, 13, 074009, https://doi.org/10.1088/1748-9326/aac939, 2018.

Zhu, Q., Peng, C., Chen, H., Fang, X., Liu, J., Jiang, H., Yang, Y., and Yang, G.: Estimating global natural wetland methane emissions using process modelling: spatio-temporal patterns and contributions to atmospheric methane fluctuations: Global natural wetland methane emissions, Global Ecology and Biogeography, 24, 959–972, https://doi.org/10.1111/geb.12307, 2015.

Zhu, Q., Iversen, C. M., Riley, W. J., Slette, I. J., and Vander Stel, H. M.: Root traits explain observed tundra vegetation nitrogen uptake patterns: Implications for trait-based land models: Tundra N Uptake Model-Data Comparison, Journal of Geophysical Research: Biogeosciences, 121, 3101–3112, https://doi.org/10.1002/2016JG003554, 2016.

Zhu, Q., Peng, C., Ciais, P., Jiang, H., Liu, J., Bousquet, P., Li, S., Chang, J., Fang, X., Zhou, X., Chen, H., Liu, S., Lin, G., Gong, P., Wang, M., Wang, H., Xiang, W., and Chen, J.: Interannual variation in methane emissions from tropical wetlands triggered by repeated El Niño Southern Oscillation, Global Change Biology, 23, 4706–4716, https://doi.org/10.1111/gcb.13726, 2017.

Zhuang, Q., Melillo, J. M., Kicklighter, D. W., Prinn, R. G., McGuire, A. D., Steudler, P. A., Felzer, B. S., and Hu, S.: Methane fluxes between terrestrial ecosystems and the atmosphere at northern high latitudes during the past century: A retrospective analysis with a process-based biogeochemistry model, Global Biogeochemical Cycles, 18, https://doi.org/10.1029/2004GB002239, 2004.